Applied Surface Science 643 (2024) 158650

Contents lists available at ScienceDirect

Applied Surface Science

journal homepage: www.elsevier.com/locate/apsusc

Full Length Article

Porous block polymer composite membranes for uranium uptake

Xinping He [a,b,c], Michael P. Dugas [e], John N. Hodul [d], Bryan W. Boudouris [d,c,*], William A. Phillip [e,*]

[a] School of Chemical Engineering and Technology, Xi'an Jiaotong University, Xi'an 710049, China
[b] The State Key Laboratory of Chemical Engineering, Department of Chemical Engineering, Tsinghua University, Beijing 100084, China
[c] Charles D. Davidson School of Chemical Engineering, Purdue University, West Lafayette, IN 47907, United States
[d] Department of Chemistry, Charles D. Davidson School of Chemical Engineering, Purdue University, West Lafayette, IN 47907, United States
[e] Department of Chemical and Biomolecular Engineering, University of Notre Dame, Notre Dame, IN 46556, United States

ARTICLE INFO

Keywords:
Block polymer composite membranes
Uranium adsorption
Amidoxime ligand
Polystyrene-b-poly(acrylic acid)

ABSTRACT

Adsorptive membranes are an effective solution to capture uranium from seawater and contaminated water supplies. Current fibrous membrane-based sorbents suffer from a low density of binding ligands at the solid–liquid interface and broad pore size distributions. These issues lead to problems such as low binding capacity and gradual breakthrough curves during flow-through adsorption. We sought to address these challenges by developing highly permeable (i.e., $\sim 3.5\times10^4$ L m^{-2} h^{-1} bar^{-1}) amidoxime-functionalized polysulfone(Psf)/polystyrene-*b*-poly(acrylic acid) (PS-PAA) composite membranes. A surface-segregation and vapor-induced phase separation (SVIPS) method was used to fabricate membranes that have an interconnected pore structure with PAA-lined pore walls. The PAA brushes offer a high density of reactive carboxyl sites that enable the surface chemistry to be modified with nitrile groups and then converted to amidoxime (AO) ligands for high-capacity uranium adsorption. The functionalized Psf/PS-PAO membrane removes uranium from dilute solution with a capacity of 150 mg g^{-1}. Flow-through experiments demonstrate rapid mass transfer of the membranes, which adsorb over 90% of the uranyl ions from flowing solutions at feed concentrations of 0.1 and 1.0 mg L^{-1}. Batch sorption–desorption experiments also indicate reusability of membranes over several cycles. Therefore, this membrane-based sorbents offers a chemically tailored platform for high-efficient uranium capture under trace concentrations.

1. Introduction

Nuclear power is one of the most promising, affordable, and low-carbon energy resources that could address the worldwide energy demand [1]. As the core fuel source of nuclear energy, uranium is the most frequently used radioactive element for nuclear power. Conventionally, uranium is gathered from terrestrial ore reserves (i.e., mainly U_3O_8) located at specific geographic regions around the globe [2]. However, due to the rise of the global energy demand, the need for nuclear power is predicted to double by 2050 [3]. This demand has forced the nuclear industry to explore other sources of uranium. Compared with terrestrial reserves, the most abundant source of uranium lies in seawater (i.e., mainly $[UO_2(CO_3)_3]^{4-}$) at an amount of 4 billion tons, which is roughly 1,000-fold that of terrestrial ores [1]. However, the concentration of uranium in seawater is, on average, 3.3 ppb [4–6]. Thus, establishing technologies for uranium capture from dilute seawater could help to create a long-term energy security solution.

Research related to uranium capture has been ongoing for almost 70 years [6]. Thus, a variety of physical and chemical separation methods, including solvent extraction [7,8], coagulation/precipitation [9,10], adsorption [11–13], and membrane filtration [14,15], have been used to recover uranium from aqueous solutions. Nevertheless, for liquid–liquid extraction, the use of organic solvents presents issues due to the generation of waste streams that must be disposed of in a safe manner [7,8,16]. As for precipitation-based methods, possible drawbacks such as a relatively low enrichment factor, production of toxic sludge, and the additional requirement for pre/post-treatments are still barriers for its large-scale application [9]. Adsorption is an alternative uranium capture method [17]. Over the past 50 years, adsorbents have advanced from the initial generation of inorganic materials such as hydrous titanium dioxide [18,19] to synthetic chelating polymers (i.e., amidoxime-,

* Corresponding authors at: Department of Chemistry, Charles D. Davidson School of Chemical Engineering, Purdue University, West Lafayette, IN 47907, United States (B.W. Boudouris).
E-mail addresses: boudouris@purdue.edu (B.W. Boudouris), william.a.phillip.1@nd.edu (W.A. Phillip).

https://doi.org/10.1016/j.apsusc.2023.158650
Received 4 May 2023; Received in revised form 30 September 2023; Accepted 8 October 2023
Available online 10 October 2023

Nomenclature

Psf	Polysulfone
PS-PAA	Polystyrene-b-poly(acrylic acid)
Psf/PS-PAA	Polysulfone/polystyrene-b-poly(acrylic acid) composite membranes
Psf/PS-PAN	Nitrile functionalized Psf/PS-PAA membranes
Psf/PS-PAO	Amidoxime functionalized Psf/PS-PAA membranes
PAN	Nitrile functionalized PAA brush
PAO	Amidoxime functionalized PAN brush
SVIPS	Surface-segregation and vapor-induced phase separation
NIPS	Non-solvent induced phase separation
VIPS	Vapor-induced phase separation
COF	Covalent organic framework
MOF	Metal–organic framework
NF	Nanofiltration
RO	Reverse osmosis
DI water	Deionized water
EDC·HCl	*N*-(3-dimethylaminopropyl)-*N*'-ethylcarbodiimide hydrochloride
NH_2OH·HCl	Hydroxylamine hydrochloride
HoBt	1-hydroxybenzotriazole hydrate
KOH	Potassium hydroxide

anthraquinone-, and calixarene-based macromolecules) [20–23] and recently to highly porous/nanostructured materials like metal organic frameworks (MOFs) [3,24] and covalent organic frameworks (COFs) [25]. Among them, amidoxime-functionalized materials are one of the most investigated materials as they have favorable binding with uranyl ions. For example, Lin et al. developed a porous uranium-targeted MOF adsorbent by functionalizing UiO-66 with amidoxime groups, which showed promising performance with a uranium adsorption capacity as high as 134 mg g^{-1} [26]. Moreover, Liu et al. reported the preparation of amidoxime-based nylon-66 fibers for uranium recovery from dilute aqueous solution, which demonstrated high removal ratio over 90 % [27]. Despite these excellent efforts using amidoxime chemistry, the powder/fiber-based adsorbent materials often lead to problems, such as agglomeration and a corresponding loss in the number of accessible adsorption sites (capacity loss), excessive pressure drop, poor mechanical strength, and difficulty in separating the adsorbent from solution for reuse. These drawbacks hinder their deployment in flow-through systems during uranium capture [28,29].

Uranium and its complex derivatives can also be efficiently captured through membrane processes such as nanofiltration (NF) [15] and reverse osmosis (RO) [30]. The advantages of NF and RO are the relatively large uranium removal ratios (>90 %) and mature membrane modules designs that promote mechanical integrity and enables their application in practical environments. Additionally, membranes are a prevalent technology on the industrial scale for metal ion filtrations [31,32]. However, the high required operating pressure (~1 MPa), energy consumption, low ion-ion selectivity, and permeability are all potential limitations to be considered when implementing pressure-driven NF and RO membrane processes, especially for uranium separation at dilute concentrations.

To address these issues, researchers have used porous membranes as adsorbents for the removal and/or detection of metal ions [33]. Relative to traditional fixed bed systems, adsorptive membrane processes force the entirety of the solution to permeate through the pores where the binding functional groups are immobilized. Because these pores range from 10 nm to 1,000 nm in diameter, they dramatically shorten the diffusion distance between target molecules and adsorption sites, showing potential for rapid separation with high throughput [34]. Furthermore, based on the commercially available materials in membrane preparation and the developed technique in both module design and fouling control (e.g., backpressure flushing), the large-scale implementation of adsorptive membranes offers the potential for an effective approach to harvest uranium with short time scales. When compared with NF and RO, adsorptive membranes usually have larger pore diameters and a corresponding lower mass transfer resistance, which then help reduce the operating pressure (approximately from 1 MPa to 0.1 MPa). By using careful molecular design (with easily tailored groups like –COOH or $–NH_2$ at the exterior of the pores), the membrane pore walls can be modified post-synthetically with a variety of functional groups that empower their use as detection and gating barriers for targeted contaminating ions [33,35]. However, uranium capture performance of state-of-art adsorptive membranes is still hindered by low saturation capacities (less than 100 mg g^{-1}) and diffuse breakthrough curves (usually take more than several hours to reach saturation [36]). Most adsorptive membranes were prepared by pre/post-grafting of functional brushes (amidoxime-based binding sites) onto nano/micro fibers to utilize their high surface area and improve the uranium adsorption capacity. Nevertheless, amidoxime-functionalized fibrous membranes are usually characterized with poor mechanical strength and wide pore size distributions, which were not compatible to be used in dynamic flow-through systems (low dynamic binding capacity and diffuse breakthrough curve) [36,37]. In view of this, there is still a need to develop an ideal adsorptive membrane which presents both high density of functional brushes and reasonable pore structures to enable efficient uranium capture from dilute solutions.

Considering the promising benefits that adsorptive membranes have to offer, polysulfone-based membranes functionalized with an amidoxime-containing block copolymer, polystyrene-*b*-poly(amidoxime) (PS-PAO), were prepared here for a uranium capture target. Polysulfone (Psf) membranes containing polystyrene-*b*-poly(acrylic acid) (denoted as Psf/PS-PAA membranes) were prepared utilizing a previously reported surface-segregation vapor-induced phase separation (SVIPS) protocol [35]. This technique enabled carboxyl group functionalities to line the pore walls of the membrane. In addition to providing tailored pore wall chemistries, the Psf/PS-PAA membranes provided high permeability (i.e., ~5.8×10^3 L m^{-2} h^{-1} bar^{-1}) relative to other membranes in the field. The PAA brushes on the pore wall of Psf/PS-PAA membranes were then functionalized with diaminomaleonitrile through carbodiimide coupling to introduce nitrile groups (–CN) and achieve Psf/PS-PAN membranes. Then, the –CN groups on membrane pore walls were further converted to amidoxime groups through a reaction with NH_2OH·HCl to generate the final Psf/PS-PAO membranes. Both membranes (Psf/PS-PAA and Psf/PS-PAO) were systematically characterized and evaluated on permeability and uranium uptake performance. Furthermore, these membranes were tested under varied pH and simulated seawater conditions to evaluate practical adsorption performance. The Psf/PS-PAO membranes had a high permeability of ~ 3.7×10^4 L m^{-2} h^{-1} bar^{-1} as well as uranium adsorptive capacity at ~ 150 mg g^{-1}. This block polymer-containing membrane allows for a proof-of-concept, feasible functionalization, and a practical uranium capture alternative to current capture methods. Thus, this platform offers an easily functionalized, low-cost, scalable, and reusable adsorptive membrane for uranium capture at trace concentrations.

2. Experimental

2.1. Materials

The PS-PAA block polymer was supplied by Polymer Source Inc. (Product ID: P18030A-SAA) with $M_n = 83.5$ kg mol^{-1}, $f_{PS} = 88.5$ %, and $Đ = 1.1$; $M_n(PS) = 70.5$ kg mol^{-1},. Polysulfone (M_n ~ 22 kg mol^{-1}), diaminomaleonitrile, 2-pyrrolidinone, *N*-(3-dimethylaminopropyl)-*N*'-ethylcarbodiimide hydrochloride (EDC·HCl), hydroxylamine hydrochloride (NH_2OH·HCl), 1-hydroxybenzotriazole hydrate (HoBt), sodium

bicarbonate ($NaHCO_3$), sodium carbonate (Na_2CO_3), potassium hydroxide (KOH), methanol, and nitric acid (HNO_3) were purchased from Sigma-Aldrich. These reagents were used directly without further purification. Deionized (DI) water was obtained through a Milli-Q water system from Millipore Inc.

2.2. Membrane preparation

2.2.1. Preparation of the Psf/PS-PAA membranes

The combination of block polymer surface-segregation and non-solvent vapor induced separation process (SVIPS) was used to fabricate porous Psf/PS-PAA membranes (Fig. 1). The membrane casting solution was prepared by dissolving 8 wt% Psf and 2 wt% PS-PAA in 2-pyrrolidinone (10 wt% polymer content in the final casting solution). After stirring for 48 h at 80 ℃ and degassing at 80 ℃ for 4 h, the homogenous casting solution was cooled to room temperature and cast on clean glass substrate with doctor blade at a thickness of 300 μm. To clean the glass substrate prior to membrane casting, the glass slide was soaked in a basic solution (KOH/water, pH ~ 13) for at least 12 h, rinsed with DI water, and dried. This cleaning prevents adhesion of the membrane to the glass substrate. After casting, the membrane structure was created in two successive phase separation steps: (1) the freshly cast solution was exposed to water vapor in a humid chamber (i.e., > 90 % relative humidity, 30 ℃) for 2 min and then (2) it was immersed in DI water bath (at 30 ℃) for another 10 h to fix the membrane nanostructure in place. Finally, the block polymer-containing composite membranes were annealed in DI water at 80 ℃ for 24 h and stored in DI water before functionalization (Fig. 1 and S1).

2.2.2. Membrane functionalization via carbodiimide coupling and amidoximation

Block polymer-containing composite membranes were functionalized via two steps to introduce the amidoxime group [2,38] on the membrane walls. Psf/PS-PAA membranes were first functionalized with diaminomaleonitrile to achieve Psf/PS-PAN membranes through carbodiimide coupling. The nitrile groups in the Psf/PS-PAN membrane were then converted to amidoxime groups through a reaction with $NH_2OH{\cdot}HCl$ to generate the final Psf/PS-PAO membranes.

For the carbodiimide coupling reaction, 1 g (52 mM) carboxyl activating agent EDC·HCl and 1.68 g (125 mM) HOBt were dissolved in 100 mL DI water, and the solution pH was adjusted to 7 with $NaHCO_3$. To activate the carboxyl groups of the PAA on membrane walls, the Psf/PS-PAA membrane was immersed in the solution and stirred for 2 h. After that, 0.2 g (18.5 mM) diaminomaleonitrile was added into the solution and the reaction mixture was stirred at room temperature for 3 days to achieve Psf/PS-PAN membranes. As diaminomaleonitrile is light-sensitive, the mixture was covered with foil during reaction. The as-prepared Psf/PS-PAN membranes were thoroughly rinsed with DI water and stored in DI water before the next step.

For the amidoximation procedure, a 30 g L^{-1} NH_2OH solution was prepared by dissolving $NH_2OH{\cdot}HCl$ into a 2:3 (by volume) mixture of methanol and water. The solution was adjusted to pH 8 with Na_2CO_3. Then, the Psf/PS-PAN membrane was immersed in the $NH_2OH{\cdot}HCl$ solution, and the mixture was stirred overnight at 80 ℃ to achieve the final Psf/PS-PAO membranes. The as-prepared Psf/PS-PAO membranes were thoroughly rinsed with DI water and stored in DI water before characterization and evaluation.

2.3. Characterization

For the block polymer composite membranes, the surface chemistry was characterized using Fourier transform infrared (FTIR) spectroscopy with a Thermo Nicolet 6700 instrument. Membrane samples were dried in a vacuum oven before characterization. For all samples, data from 800 cm^{-1} to 4500 cm^{-1} were collected at a resolution of 2 cm^{-1}, and each spectrum was scanned for 32 times.

X-ray photoelectron spectroscopy (XPS) analysis was performed utilizing a Phi VersaProbe II with MultiPak software. The samples were analyzed for C, N, O, and F. The spectra were shifted based upon the location of the 286 eV C–C peak. The N1s spectrum was analyzed to investigate the progress of the reactions occurring on membrane pore walls as the acrylic acid repeat units were converted to amidoxime.

The morphologies of the membrane surface and cross-section were analyzed with Hitachi S-4800 and Helios G4 UX Dual Beam scanning electron microscopes. Cross-sectional scanning electron microscopy (SEM) samples were prepared by appropriate fracture in liquid nitrogen bath. Before imaging, both the surface and cross-section samples were dried in a vacuum oven and then coated with carbon (~20 s) (SPI sputter

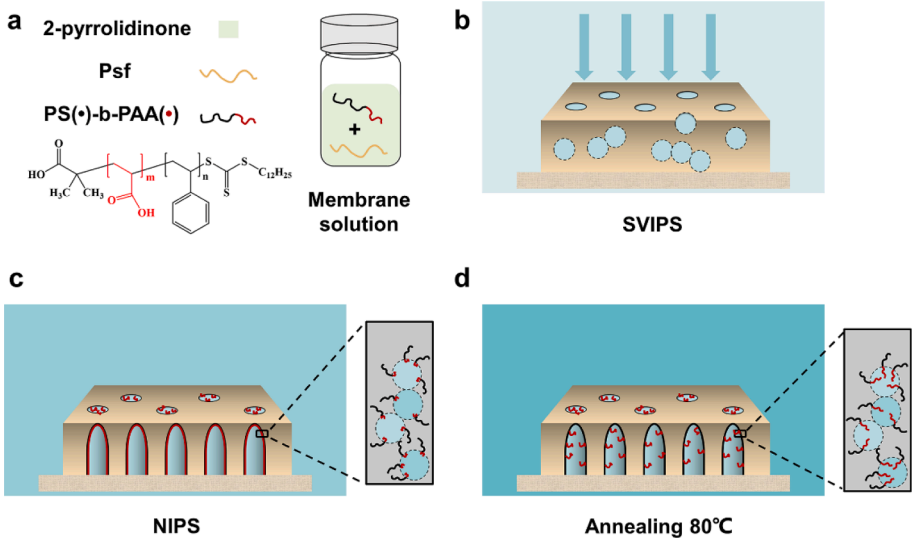

Fig. 1. Membrane fabrication through the SVIPS process. (a) The membrane solution was prepared by dissolving polysulfone (Psf) and PS-PAA in 2-pyrrolidinone. (b) The freshly cast film was first exposed to water vapor in a humidity chamber (i.e., > 90 % relative humidity, 30 ℃) for 2 min. The intrusion of water vapor into the casting solution simultaneously induced the phase separation process and the surface-segregation of PS-PAA, resulting in bicontinuous pores. (c) The nascent membrane was then solidified by quenching in the coagulation (DI water) bath. As the phase separation proceeds, the hydrophobic PS block preferentially partitions into the Psf matrix, and the hydrophilic PAA moieties accumulate at the pore walls. (d) The membrane was finally annealed in another DI water bath at 80 ℃ to bring the PAA brushes to a more extended configuration.

coater, Division of Structure Probe, Inc.) to prevent sample charging.

Pore size analysis of Psf/Ps-PAA membrane was characterized using a gas–liquid displacement method with capillary flow porometry (POROLUX 1000, POROMETER, Germany). Membrane samples were punched into 20 mm-diameter discs and immersed in porefil (low vapor pressure reagent with surface tension at 16 dyn cm^{-1}) to ensure all pores are filled. When all the membrane pores were wetted, the membrane was subjected to increasing pressure (supplied by pure nitrogen) until porefil was totally expelled. The pressure change for both wet and dry samples were recorded, and then the pore-size distribution was calculated based on Young-Laplace equation.

2.4. Evaluation of permeability and uranium adsorption

The membranes were punched into 2.5 cm-diameter discs for evaluation in an Amicon 8010 stirred cell. A polyethylene non-woven fabric was used as support substrate during testing. Permeability under varied pH and pressure conditions were collected for both the Psf/PS-PAA and Psf/PS-PAO membranes.

To investigate the adsorption performance of the Psf/PS-PAA membranes and the functionalized Psf/PS-PAO membranes, uranyl nitrate hexahydrate solutions of varied concentrations (0 mg L^{-1}, 5 mg L^{-1}, 10 mg L^{-1}, 15 mg L^{-1}, 25 mg L^{-1}, 50 mg L^{-1}, and 100 mg L^{-1}) were prepared as feed solutions. Specifically, for the adsorption test, membrane samples were immersed in uranyl nitrate solutions (10 mL in varied concentrations) for 24 h. Then, all the membrane samples were rinsed with DI water and dried with wipes before they were released in 1 M HNO_3 solution (10 mL) for another 24 h. Finally, concentrations for all the retained and releasing solutions were analyzed with a Perkin Elmer Avio 200 inductively coupled plasma optical emission spectrometer (ICP-OES).

Competitive adsorption and cycling experiments were conducted to determine the selectivity of the membranes to uranium as well as the reusability of the membrane. Simulated sea water containing 10.5 mM Ca^{2+}, 480 mM Na^{+}, 10.2 mM K^{+}, 54.5 mM Mg^{2+}, 561 mM Cl^{-}, 2.4 mM HCO_3^{-}, 28.4 mM SO_4^{2-} was prepared with pH at 8.26[35]. For the competitive adsorption experiments, 10 mg L^{-1} each of copper chloride and uranyl nitrate was dissolved in 10 mL of simulated sea water, in which the membrane samples were immersed and allowed to equilibrate for 24 h. The membranes were then rinsed in DI water, lightly patted dry, and allowed to release in 1 M HNO_3 solutions. For the regeneration and reuse experiments, the samples were submerged in 10 mL simulated sea water solutions containing 1 mg L^{-1} uranyl ions. The membranes were allowed to equilibrate for at least 24 h. The membranes were then rinsed in DI water, dried with a laboratory wipe, and submerged in 1 mL of the HNO_3 release solution. After the release, the membrane was rinsed again with DI water and allowed to soak in DI water for 24 h. Then, the samples were resubmerged in the simulated sea water feed solution. For both experiments, the concentrations for the remaining and release solutions were analyzed with a Perkin Elmer Optima 8000 Prep 3 ICP-OES.

Flow-through experiments were conducted to determine the dynamic sorption capabilities of the membranes. Membranes were placed in an Amicon 8010 stir cell along with 10 mL of either 0.1 ppm or 1 ppm uranyl ion aqueous solutions as the feed solution. The membranes were then allowed to permeate the solution gravimetrically, and the permeate was collected in ~ 1 g interval until the entire solution had permeated the membrane. The membranes were then rinsed in DI water, dried with a laboratory wipe, and submerged in the HNO_3 release solution. The release solution, along with the collected permeate solutions, were analyzed on a Perkin Elmer Optima 8000 Prep 3 ICP-OES.

3. Results and discussion

3.1. Preparation and functionalization of Psf/PS-PAA membranes

3.1.1. Preparation of Psf/PS-PAA membranes

A bi-continuous porous structure is an important feature during the preparation of adsorptive membranes, especially if high capacity and permeability are target metrics of the end-use application. The accessibility associated with the interconnected pore structure yields pore walls that are easier to functionalize for the targeted capture of dissolved species (i.e., uranium in this effort). To achieve the desired morphology, SVIPS was applied to prepare porous block copolymer membranes [35,39].

In the conventional non-solvent induced phase separation (NIPS) method for membrane preparation, spinodal decomposition dominates the phase separation process. During the spinodal decomposition process, exchange rates between solvents and non-solvents can be high, resulting in a steep concentration gradient across the cross-section of the cast polymer solution. Therefore, membranes prepared by the NIPS method often present asymmetric morphologies with a skin layer possessing small pores forming on the top surface near the interface between the non-solvent bath and cast solution. This structure transitions into a highly porous structure with large pores across the membrane thickness [40]. Compared with NIPS, VIPS (vapor induced phase separation) is generally characterized by relatively slow nonsolvent vapor exchange rates in which the mechanism of nucleation and growth dominates the phase separation process[39]. In this work, both SVIPS and NIPS process were used for membrane preparation (Fig. 1). Specifically, water vapor was used as nonsolvent in the beginning to induce SVIPS for a fixed period of time and then the nascent membrane was solidified by quenching in the DI water coagulation bath through NIPS. Due to the slow transport (compared with liquid–liquid de-mixing) of water vapor into polymer solution, the polymer-lean phase had longer time to grow or coalescence before the solidification of polymer-rich phase, which then lead to the formation of large-pore structure and interconnected morphologies for both Psf and Psf/PS-PAA membranes [41].

It is apparent that both the surface and cross-sectional views of the composite Psf/PS-PAA membranes present more pores relative to the homopolymer (Psf) membranes, which is primarily ascribed to the surface-segregation ability of PS-PAA during phase separation [42,43]. Specifically, for the Psf/PS-PAA membranes, the intrusion of water vapor into the casting solution simultaneously promotes the VIPS process and the surface-segregation of PS-PAA to the interface between polymer and nonsolvent. As the VIPS proceeds, the hydrophobic PS block preferentially partitions into the Psf matrix, and the hydrophilic PAA moiety accumulates at the pore walls. This increases the hydrophilicity of pore walls and accelerates the nonsolvent-solvent exchange rate compared with Psf homopolymer membrane. The higher exchange rate then leads to a rapid vitrification of the Psf/PS-PAA membranes, which then have pores (diameters ranging from 0.3 μm to 3 μm) kinetically trapped in place before the coalescence of polymer-rich phase (Fig. 2d) [44]. The pore size distribution of Psf/Ps-PAA membranes was also analyzed through capillary flow porometry (POROLUX 1000, POROMETER, Germany). Results show that the Psf/Ps-PAA membranes present a narrow pore size distribution with an average pore diameter of 2.18 μm (Figure S2). For the Psf casting solution, however, the nonsolvent-solvent exchange rate is lower compared with Psf/PS-PAA solution due to the lack of polar PAA units. As a result, the polymer-lean phase and polymer-rich phase tend to coalesce due to interfacial tension (Fig. 2b) [45]. This physical picture provides a rationale for the morphology difference between the polysulfone and Psf/PS-PAA membranes. The water contact angles were measured to assess the hydrophilicity of membranes. Results indicated that water contact angle for pure Psf membrane and Psf/PS-PAA membrane is around 110.2° and 88.2° respectively (Table S1), which again proved

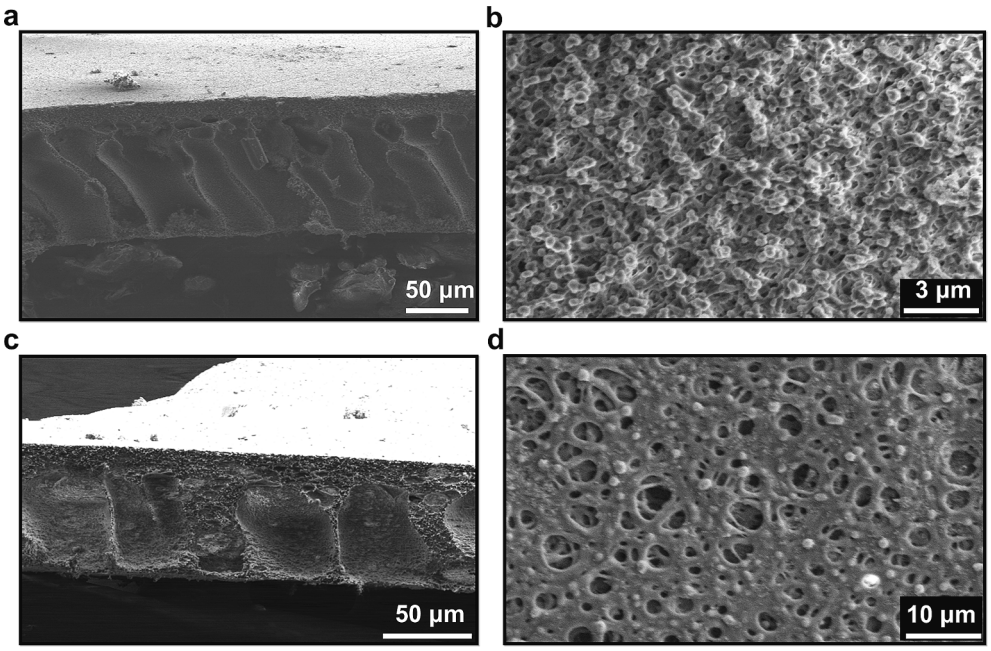

Fig. 2. (a-b) Homopolymer Psf membranes and (c-d) composite Psf/PS-PAA membranes prepared through a SVIPS technique, where newly cast solutions were exposed to humid air (>90 % relative humidity) for 2 min and then immersed in the DI water bath to fix the microstructure in place. With the slow phase separation and delayed de-mixing of the SVIPS process, the cross-sections of both (a) Psf membrane and (c) Psf/PS-PAA membrane possessed an asymmetric morphology with a spongy porous layer at the upper surface (i.e., close to non-solvent/solution interface) and a finger-like layer at the bottom. (b) The surface morphology of the Psf membranes showed microscale pores and the coalescence of polymer-rich phase due to relatively slower nonsolvent/solvent mass-transfer rates. (d) The surface morphology of composite Psf/PS-PAA membranes showed microporous structure with a higher density of bicontinuous pores.

the increased hydrophilicity of Psf/PS-PAA membrane (based on the migration of PAA chain onto the pore surface).

Both Psf (Fig. 2a) and Psf/PS-PAA (Fig. 2c) membranes showed an asymmetric morphology typical of SVIPS-cast membranes. The cross-sectional views consisted of a spongy porous layer around 15 μm in depth near the upper surface and a finger-like porous layer at the bottom surface. Specifically, the top spongy layer was ascribed to the slow phase separation in humidity chamber (VIPS), while the finger-like pores were resulted from the fast phase separation in the DI water bath (NIPS).

In addition to the interconnected pore structures, the SVIPS casting process generates membranes that are amenable to post-casting functionalization of the pore walls [35].

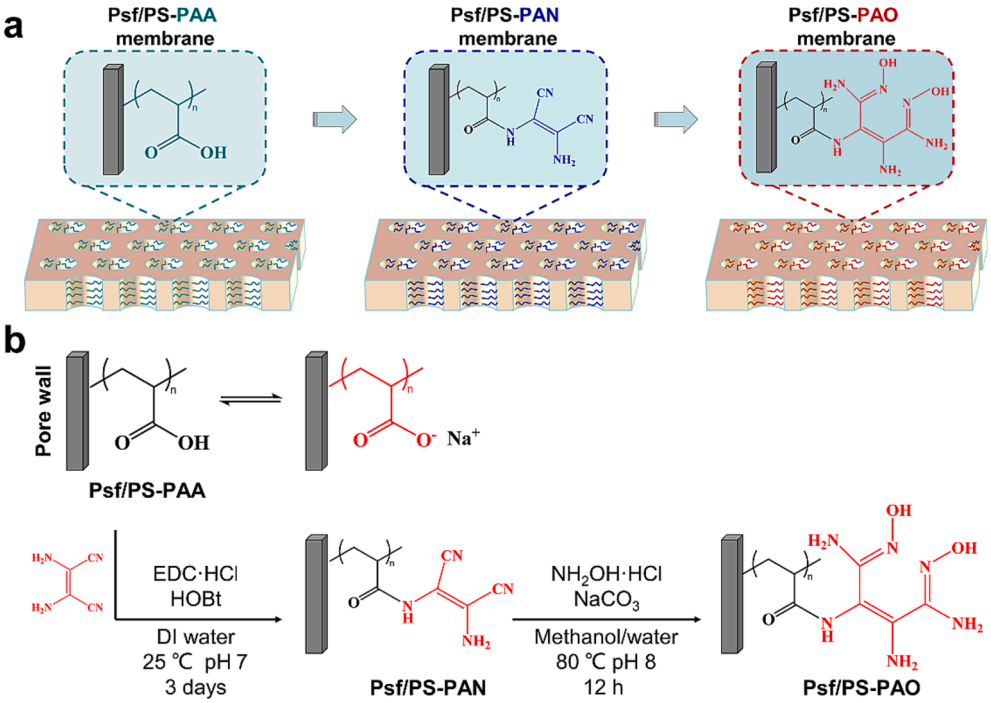

Fig. 3. (a) Illustration and (b) functionalization scheme for the preparation of Psf/PS-PAO membranes starting from the parent Psf/PS-PAA membranes.

3.1.2. Functionalization of Psf/PS-PAA to Psf/PS-PAO membranes

The PAA chains are more likely to reside along the pore wall exposed to the aqueous phase, which makes the subsequent functionalization reaction easy to push towards high conversion. The sequential functionalization scheme of Psf/PS-PAO membrane is outlined in Fig. 3. The first step is to graft diaminomaleonitrile onto the membrane pore walls through carbodiimide coupling to introduce nitrile groups. Then, these nitrile groups were transformed to amidoxime groups to enable the efficient bonding between uranium and membranes. The carbodiimide coupling is a slow reaction in which longer reaction times (i.e., several days) are normally required at room temperature. For the amidoximation reaction, conversion of PS-PAN to PS-PAO is usually greater than 80 % when the temperature is 80 ℃ [46].

As shown in the FTIR spectra (Fig. 4; full spectrum is available in Figure S3), evidence of a successful carbodiimide coupling reaction on the membrane surface is provided by the shift of the C=O peak from around 1680 cm^{-1} (representing the carboxyl dimer) to 1630 cm^{-1} (indicative of the formation of amide), which suggests the formation of an amide bond as the PS-PAA is converted to PS-PAN. Meanwhile, the typical peak for the stretching vibration of the cyano group of Psf/PS-PAN membranes is around 2210 cm^{-1}. This vibration, however, disappeared in the Psf/PS-PAO membranes, which indicates the successful reaction of both carbodiimide coupling with diaminomaleonitrile and amidoximation utilizing hydroxylamine. In addition, the peak around a wavenumber of 1650 cm^{-1} is associated with the C=N of the amidoxime group, which is consistent with the coupling of the amidoxime moiety on the membranes [12].

XPS analysis was conducted to further ensure the reaction products as the PAA side chains segregated on the membrane pore wall were successfully converted to amidoxime-functionalized PAO (Fig. 3). Figure S4 shows the XPS N1s spectra for each step in the reaction scheme. The parent Psf/PS-PAA membrane, as seen in Figure S4a, shows one large peak at 400.5 eV. This peak is attributed to some contamination as neither the Psf matrix nor the PS-PAA copolymer contain nitrogen in their structure and will not be incorporated into the analysis. Figure S4b shows the N1s spectrum for the Psf/PS-PAN functionalized membrane. The peaks at 398.7 eV correspond with the primary amines (NH_2). Peaks at 402 eV correspond with the secondary amines (NH) and nitriles[47]. The presence of these peaks suggested that the carbodiimide coupling reaction was successful. Figure S4c displays the N1s spectrum for the Psf/PS-PAO functionalized membrane. Two peaks are seen in the spectrum which correlate to the primary amine (399 eV) and the oxime (401 eV, C=NOH) functionalities[48]. The XPS results further suggest a successful reaction from acrylic acid to amidoxime functionalities.

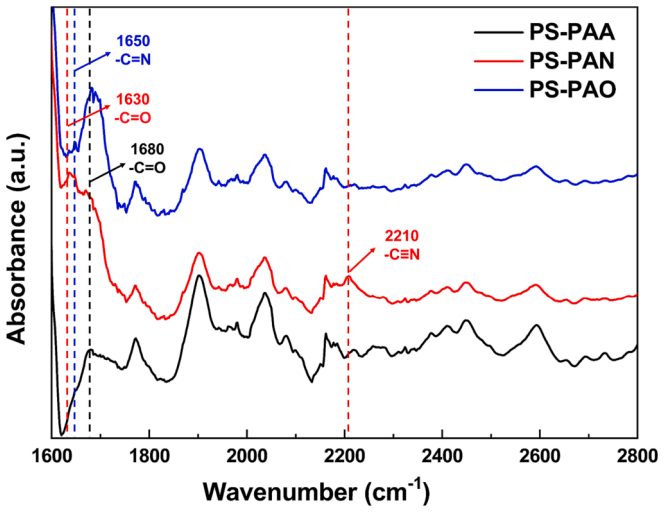

Fig. 4. FTIR spectra of Psf/PS-PAA membranes and functionalized Psf/PS-PAN and Psf/PS-PAO membranes. The spectra are reported for wavenumbers from 1600 cm^{-1} to 2800 cm^{-1}. Peaks around 1630 cm^{-1} and 1680 cm^{-1} represent the C=O from amide and carboxyl dimer. The appearance of the peak at 1650 cm^{-1} are consistent with the formation of amidoxime in the Psf/PS-PAO membranes. The peak at 2210 cm^{-1} suggests the appearance of –CN groups in the Psf/PS-PAN membranes.

After functionalization, the morphologies of the Psf/PS-PAN and the Psf/PS-PAO membranes (Fig. 5) did not show any appreciable structural change in comparison to the Psf/PS-PAA membrane. Both the Psf/PS-PAN and Psf/PS-PAO membranes showed clear interconnected open pores on the surfaces and asymmetric morphologies on cross sections resulting from SVIPS and the ensuing NIPS process.

3.2. Performance evaluation for Psf/PS-PAA and functionalized Psf/PS-PAO membranes

3.2.1. pH-responsive permeability

The pH-responsive hydraulic permeability of the Psf/PS-PAA and Psf/PS-PAO membranes were evaluated. According to the pH-responsive permeability and the pore morphology, it is clear that the PAA and PAO brushes were attached to the pore walls of the membranes (Fig. 6 and Fig. 7). The permeability in DI water (pH 5.5) of Psf/PS-PAA (5.8×10^3 L m^{-2} h^{-1} bar^{-1}) and Psf/PS-PAO (3.5×10^4 L m^{-2} h^{-1} bar^{-1}) membranes also demonstrate that both membranes are highly permeable.

As shown in Fig. 7, both the Psf/PS-PAA and Psf/PS-PAO membranes had a pH-responsive permeability, exhibiting higher water flux at low pH conditions. This phenomenon is attributed to the morphology changes of the PAA and PAO brushes along the pore walls [49,50]. With Psf/PS-PAA and Psf/PS-PAO membranes exposed to a pH = 1.66 solution, the protonated carboxylic acid groups and oxime groups in PAA and PAO form hydrogen bonds with other moieties, which leads to a relatively collapsed chain morphology and thus higher effective pore diameter and higher permeability. In contrast, when exposed to a pH = 12.16 solution, both carboxyl groups in PAA and oxime groups in PAO moiety were deprotonated and electrostatically repelled each other, which leads to an extended chain morphology that decreased the effective pore diameter and resulted in a relatively lower permeability.

The permeability of the Psf/PS-PAO membranes at all pH conditions (from 3.8×10^4 L m^{-2} h^{-1} bar^{-1} at pH 12.16 to 5.1×10^4 L m^{-2} h^{-1} bar^{-1} at pH 1.66) were about an order of magnitude larger than the permeability of the Psf/PS-PAA membranes. This difference in permeability is possibly due to the conformation of the PAO brushes. First, after the functionalization from Psf/PS-PAA to Psf/PS-PAO membrane (Fig. 3), more –NH_2 and –OH groups (donor of hydrogen bond) were introduced onto membrane pore wall, which could then form inter- and intramolecular hydrogen bond with C=O nearby. The hydrogen bonds within the PAO brushes could lead to a more collapsed polymer conformation, and thus, a bigger pore size and higher permeability (Fig. 7). Second, more –NH_2 and –OH groups in PAO moiety could also help improve the hydrophilicity of membrane pore wall and then resulted in a higher permeability. Thus, with unique structure of amidoxime functionalities and more hydrophilic groups presenting on the pore walls, the Psf/PS-PAO membranes offers a highly permeable platform for implementation during uranium uptake.

3.2.2. Adsorption isotherms

Static uranium adsorption experiments of both Psf/PS-PAA and functionalized Psf/PS-PAO membranes were performed. Adsorption isotherms were assessed using aqueous uranyl nitrate solutions under varied initial feed concentration (0 mg L^{-1}, 5 mg L^{-1}, 10 mg L^{-1}, 15 mg L^{-1}, 25 mg L^{-1}, 50 mg L^{-1}, and 100 mg L^{-1}). After immersing membrane samples into the uranyl nitrate solutions and allowing the systems to equilibrate for 24 h, the concentration of uranyl ions in the solutions decreased due to adsorption onto membrane surfaces. The experimental isotherms were then obtained by plotting the adsorbed capacity of

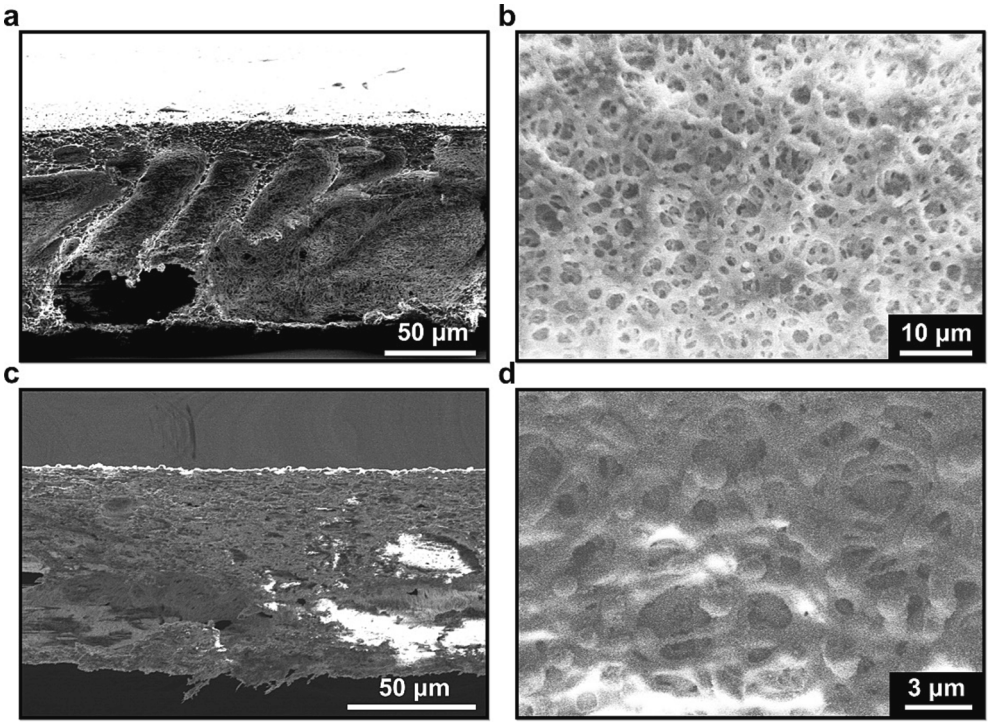

Fig. 5. Representative SEM micrograph of the (a) cross-sectional and (b) surface views of the Psf/PS-PAN membrane and the (c) cross-sectional and (d) surface views of the Psf/PS-PAO membrane.

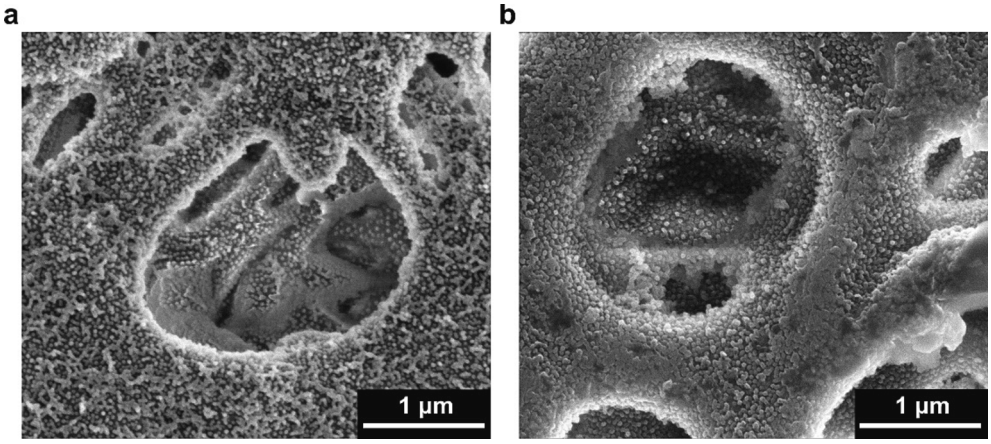

Fig. 6. (a) High resolution image of pore walls for Psf/PS-PAA membrane. The PAA brushes uniformly lined the inner and outer surface of membrane pores, which enabled the high-efficient utilization of membrane pores to be further functionalized with ligands for the adsorption of the target solute. (b) High resolution image of pore walls for Psf/PS-PAO membrane. The PAO brushes also uniformly lined the membrane pore walls. Compared with the PAA brushes, the conformation of PAO was more contracted, which should be ascribed to more inter- and intramolecular hydrogen bonds in PAO moiety.

uranyl ions against the equilibrium concentrations of uranyl ions in solution. Isotherms (Fig. 8) of both membranes show a linear increase in adsorbed capacity as a function of the final uranyl concentration in feed solutions. To further quantify the adsorption information of Psf/PS-PAA and functionalized Psf/PS-PAO membranes in aqueous uranyl nitrate solutions, different isotherm models were used, and the model parameters were estimated using nonlinear regression[51]. According to the linear shape and the fitting results of isotherms, both Psf/PS-PAA and Psf/PS-PAO membrane sorbents are in the linear regime and not fully saturated under the solution concentrations examined.

The experimental data reported in Fig. 8 for the Psf/PS-PAA and Psf/PS-PAO membranes exhibit behavior consistent with the linear regime of chemical adsorption models (i.e., the Langmuir and Volmer modules). Therefore, both models are studied here because they identify several trends that allow for a comparison of the two membrane chemistries. First, the maximum amount of uranyl ions adsorbed (Q_{max}) estimated by Langmuir model for Psf/PS-PAO and Psf/PS-PAA sorbents are approximately 77.43 mg g^{-1} and 61.80 mg g^{-1}. Based on the Volmer model, Q_{max} are 149.64 mg g^{-1} and 100.23 mg g^{-1} for Psf/PS-PAO and Psf/PS-PAA sorbents, respectively. Therefore, both Langmuir and Volmer models suggest a higher capacity of Psf/PS-PAO membrane sorbents for uranyl adsorption. The higher capacity of Psf/PS-PAO membrane sorbents could be ascribed to the pore wall functionalities. Specifically, the amidoxime group mainly showed monodentate coordination binding modes with uranyl ions, while carboxyl groups usually act as monodentate or bidentate ligands[52–54]. As shown in functionalization scheme (Fig. 3), the carbodiimide coupling and amidoximation reaction would change one carboxyl group to two amidoxime groups, which

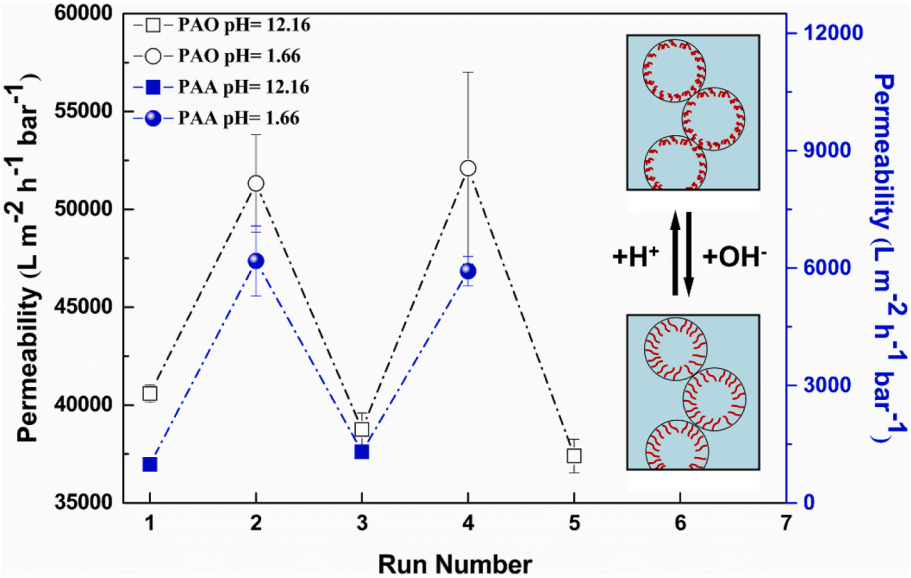

Fig. 7. Hydraulic permeability of Psf/PS-PAA and Psf/PS-PAO membranes as a function of solution pH. The permeability of membrane was measured as it was exposed to solutions that alternated between pH = 1.66 and pH = 12.16. The reversible and repeatable change in permeability under varied pH conditions was a direct result of the extension and contraction of the PAA and PAO brushes that line the pore walls (shown in the inset figure). The errors are the standard deviation from at least n = 3 membrane samples.

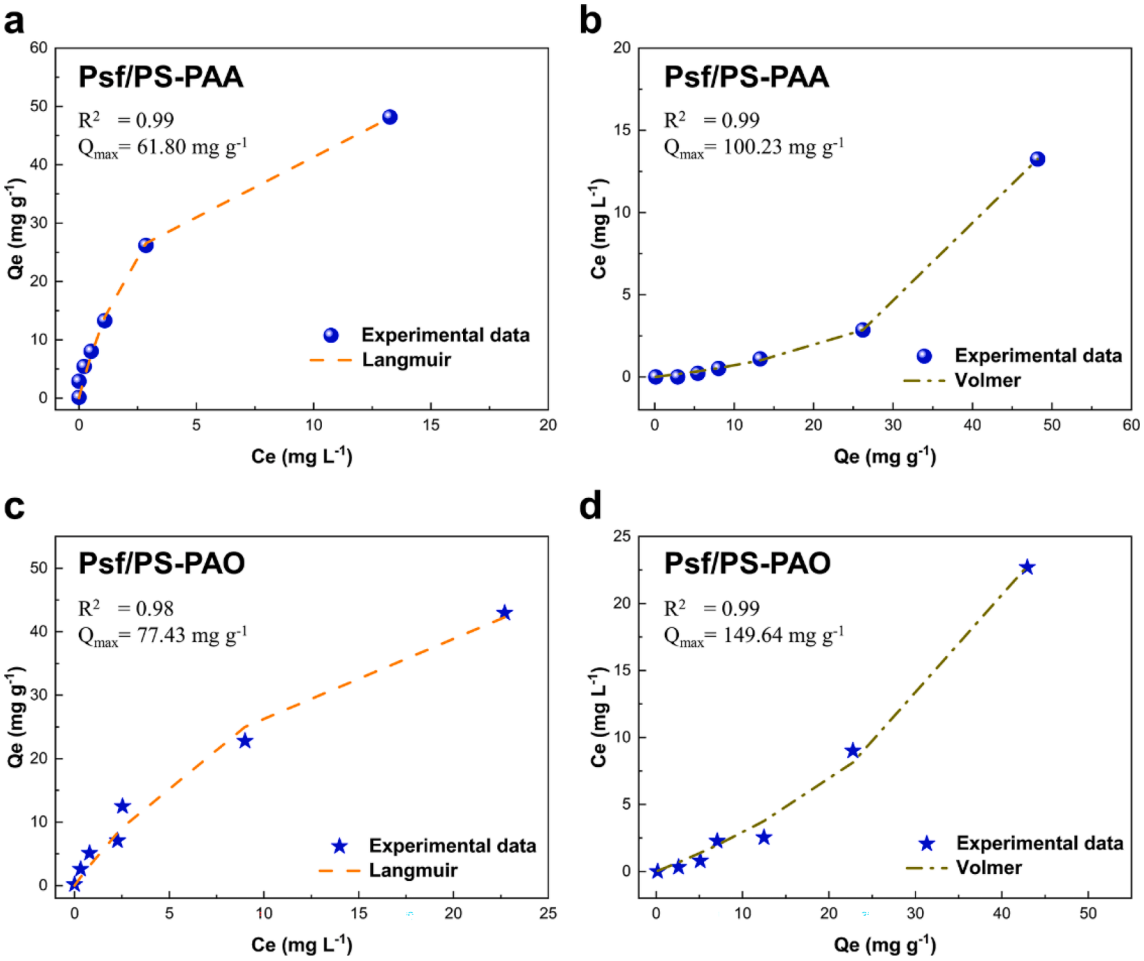

Fig. 8. Uranyl adsorption isotherms based on different isotherm models for (a-b) Psf/PS-PAA and (c-d) Psf/PS-PAO membrane sorbents. The concentration of uranyl ions bound to the membrane is reported as a function of the final uranyl concentration in feed solutions. The dashed lines through the data represent the corresponding isotherms determined from nonlinear regression. C_e represents the final concentration of solutions and Q_e represents the adsorbed concentration. R^2 is the correlation coefficient and Q_{max} is the maximum capacity estimated by different isotherm models.

could then offer more binding sites for uranyl ions and thus higher theoretical adsorption capacity.

According to the isotherm analysis, the maximum adsorption capacity of Psf/PS-PAA (~100 mg g^{-1}) and Psf/PS-PAO membranes (~150 mg g^{-1}) are comparable with many other fiber-based (~60 mg g^{-1}) absorbent materials[27,36].

3.2.3. Competitive adsorption

In practical applications, the binding events associated with the membranes will compete with the high ionic strengths and interfering ions that occur naturally within seawater. To establish the performance of the membranes under these demanding conditions, batch and flow-through experiments were conducted.

Fig. 9a shows the batch uranyl uptake for PAO functionalized membranes under DI water and synthetic seawater conditions in batch experiments. The initial feed solution uranium concentration was kept constant at 10 mg L^{-1} for each experiment. The membranes show a dramatic decrease in the uptake of uranium once the environment is changed from DI water to seawater. This decrease in the uptake could be attributed to the uranyl ion shifting to a species that does not favorably interact with the amidoxime functionality. In pH < 4 solutions, UO_2^{2+} is dominant. It is thought that the amidoxime group can act as a bidentate ligand system for the uranyl cation. The lone pairs of electrons on the oxime oxygen and the amino nitrogen are donated to the positive UO_2^{2+} center to form a five-membered ring including the metal ion. However, when solutions have pH > 8 (for instance, the pH values of seawater are usually higher than 8 [55]), uranium would be hydrolyzed to species such as $UO_2(OH)^{3-}$ and $UO_2(CO_3)_3^{4-}$, leading to the repulsion of these anions to the negatively charged membrane surface. In uptake experiments from literature, the pH was set to 4–5 [56,57], limiting the speciation of the uranyl ion to favor adsorption. However, the pH of the synthetic sea water was approximately 8.26, which makes the repulsed uranyl species more dominant.

Competitive uranium and copper adsorption experiments in synthetic seawater (pH 8.26) were conducted to understand the selectivity of the PAO functionality to uranium. Previous work in literature has shown that several ions compete with uranyl ions to bind to the amidoxime functionalities, especially copper and vanadium [58,59]. In the current manuscript, copper was used as competing ions to represent other transition metal ions that has shown to bind with the acrylic acid and/or amidoxime moieties from the parent copolymer. In these experiments, the copper and uranyl ion concentration of the initial feed solution was 10 mg L^{-1}. Fig. 9b shows the uptake of both uranium and copper with PS-PAA and PS-PAO functionalized membranes in batch experiments with synthetic seawater. For both the PAA and PAO functionalities, copper ions bind more readily than uranyl ions. This phenomenon could be due to the shift in uranyl speciation discussed previously, limiting the adsorption. While copper also shifts to a hydroxide form at the pH of seawater, the conversion to a neutral species is less pronounced, allowing for more copper (5–10 %) to maintain a positive charge[60], and therefore be electrostatically attracted to the negatively charged functionalities.

Results in Fig. 9 indicate that the performance of uranyl ion adsorption suffers a little when membrane sorbents are exposed to alkaline synthetic seawater or solutions with competing ions. Nevertheless, as more promising molecular recognition moieties are identified, they can be covalently bound to the Psf/PS-PAA membrane-based sorbent such that it can achieve its full potential towards uranyl ion adsorption under trace concentrations.

3.2.4. Dynamic flow-through experiment

Membrane-based sorbents often exhibit rapid mass transfer characteristics to capture target solutes from solution effectively. Flow-through experiments were conducted to determine the adsorption capability of the Psf/Ps-PAO membranes while solution is flowing convectively. The flux through the membrane was controlled to approximately 5900 L m^{-2} h^{-1}, which is equivalent to a superficial velocity of 1.6 mm s^{-1}. Fig. 10a shows uptake results for both the 0.1 and 1.0 mg L^{-1} feed solutions. In each experiment, 10 mL of solution was permeated through the membrane and captured in approximately 1 mL intervals (Figure S5). The membranes are able to adsorb over 90 % of the uranyl ions from the flowing solution, regardless of the initial feed concentration (0.1 and 1.0 mg L^{-1}). The concentration of uranium in the 1 mL aliquots of permeate that were collected over the course of the experiment stays below the detection limit for the 0.1 ppm experiments. For the 1.0 ppm experiments, a slight increasing trend can be observed throughout the experiment. However, well over 90% of the uranium is adsorbed onto the membrane, as evidenced by the low uranium concentration in the permeate.

The results from flow-through experiments can be used to understand the kinetic behavior of the Psf/Ps-PAO membranes for uranium capture. The adsorption of uranyl ions onto the membrane during the flow through experiments indicates that the kinetics are limited by the ions diffusing to the membrane pore wall rather than the uranyl ion binding to the amidoxime functionality. In each experiment, 10 mL of solution was permeated through the membrane with the flux controlled to around 5900 L m^{-2} h^{-1}. The area of the membrane (5.07×10^{-4} m^2) was multiplied by the porosity (86 %) to show a total pore area of 4.36×10^{-4} m^2. Based on this area combined with permeate flow rate (6.7×10^{-4} L s^{-1}) and the assumed thickness of the membrane (~100 μm), the residence time of solution passing through the membrane was calculated to approximately 65 ms. As seen in Figure S5, the Psf/PS-PAO membranes adsorb over 90% of the uranyl ions from the flowing solution, regardless of the initial feed concentration (0.1 and 1.0 mg L^{-1}). This result indicates that, without the presence of interfering ions, the amidoxime functionalities have qualitatively fast uptake kinetics. Previous studies performed in literature support this observation, with the kinetics following a pseudo second order reaction [61,62].

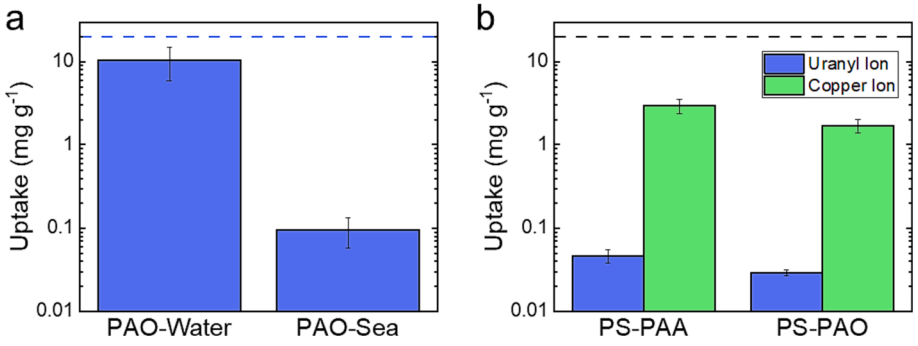

Fig. 9. (a) Uranyl ion adsorption comparison of Psf/PS-PAO functionalized membranes in DI water and in seawater. The initial uranyl ion concentration was 10 mg L^{-1} for each case. (b) 10 mg L^{-1} uranyl and copper ion competitive adsorption with Psf/PS-PAA and Psf/PS-PAO membranes in sea water. The dashed lines are the theoretical maximum uptake of uranyl ion from the solution mass balance. The errors are the standard deviation from n = 5 membrane samples.

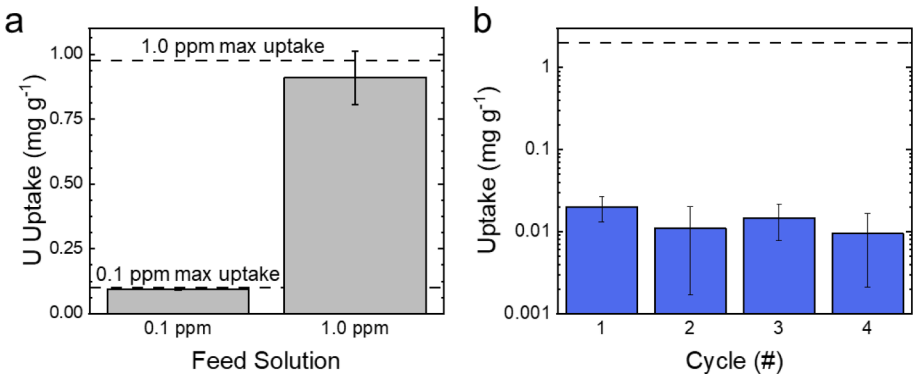

Fig. 10. (a) Flow-through adsorption uptakes of uranyl ions with 0.1 and 1.0 mg L^{-1} aqueous feed solutions. The superficial velocity was held at 0.16 cm s^{-1}, and 10 mL of solution was permeated through each membrane. The errors are from n = 2 experiments (b) Cycling 1.0 mg L^{-1} uranyl ion uptakes in seawater. These results were from batch experiments where the membrane was subject to 10 mL of solution each cycle. The errors are from n = 4 samples. The dashed lines are the maximum theoretical uptakes for each condition.

The saturation time (under dynamic flow) for the membrane would depend on the concentration of the uranyl solution, the flow rate of solution through the membrane, and the mass of the membrane material. According to the dynamic flow-through experiment, the Psf/PS-PAO membrane (2.5 cm in diameter, ~18 mg in mass) adsorbed over 90 % of uranyl ions from 10 mL feed solutions within 15 s. In other words, take 1.0 mg L^{-1} of feed uranyl solution as an example, the Psf/PS-PAO membrane adsorb ~ 0.009 mg uranyl ions from 10 mL feed in 15 s (0.6 μg s^{-1}). Considering the adsorption capacity of Psf/PS-PAO membrane at a concentration of 1 mg L^{-1} is around 6.3 mg g^{-1} (from adsorption isotherm analysis), it will reach saturation after 3.1 min, or approximately 125 mL of 1.0 mg L^{-1} of feed uranyl solution, in dynamic flow through adsorption. This estimate depends strongly on the process conditions and using a higher mass of membrane would increase the saturation time.

3.2.5. *Reusability and long-term stability*

To test the reusability of the membrane, sorption–desorption cycling experiments were conducted in simulated seawater. Fig. 10b shows the results of the batch sorption–desorption experiments conducted with the PAO-functionalized membranes. The feed solutions were kept at 1.0 mg L^{-1} uranyl ion concentration. The uptake is low (~0.01 mg g^{-1}), in which is consistent with the uptake observed in the batch seawater uptake experiments. This low uptake is attributed to the species change from the pH of the seawater. However, the uptake is reproducible over several cycles.

The uptake experiments were also conducted with PAO functionalized membranes that were recently functionalized (<1 week) and compared to membranes that were aged (>1 year). As seen in Figure S6, the FTIR spectra for both membranes are identical, indicating the amidoxime functionality is stable for long periods of time. It's worth mentioning that uranium is a kind of α-emitter, and polysulfone has shown to have reasonable resistance to α radiation, which also help ensure the stability of membranes during uranium capture[63–65]. In addition, the adsorption capacities for both membranes show the same trend with water and seawater (Figure S7). Each membrane sample was subjected to 10 mL of either water or seawater with 10 mg L^{-1} uranyl ions in solution. For the older membrane, the uranium adsorption capacity in water was 10.5±4.6 mg g^{-1} while the new membrane capacity was 5.5±2.2 mg g^{-1}. The lower capacity for the newer membrane could be due to a lower density of amidoxime moieties. These results indicate that the amidoxime functionality is stable chemically, allowing uranyl ions to be adsorbed and desorbed without causing permanent harm to the uptake capacity.

4. Conclusions

A membrane-based sorbent with interconnected pore structure, high permeability and adsorption capacity was prepared through surface-segregation and vapor-induced phase separation (SVIPS) technique. The membrane fabrication was followed by straightforward and flexible covalent coupling reaction to functionalize pore walls with uranium binding moieties (amidoxime) for efficient uranium adsorption from diluted aqueous solutions. In addition to providing high hydraulic permeability (~3.5×10^4 L m^{-2} h^{-1} bar^{-1}), the functionalized Psf/PS-PAO membrane sorbents can also remove uranium from dilute solutions with a capacity of 150 mg g^{-1}. Dynamic flow-through experiments demonstrate that the Psf/PS-PAO membranes exhibit rapid mass transfer characteristics and are able to adsorb over 90 % of the uranyl ions in the solutions when exposed to convective flow, regardless of the initial feed concentrations (0.1 and 1.0 mg L^{-1}). Although the uranium adsorption performance suffers when membrane sorbents are exposed to simulated seawater or solution with competing ions, the functionalized membranes exhibit good reproducibility of sorption–desorption experiments over several cycles. Additionally, the membranes also present excellent long-term stability over 1 year for adsorption capacity, indicating the stable functionality of amidoxime and membrane structure. Based on the flexibility associated with the SVIPS and functionalization process, this block polymer-containing membrane allows for a scalable, reliable and reusable sorbent platform for membrane-based adsorption process.

In general, a real benefit of our approach is that the pore wall modification occurs after the membrane structure has been fixed in place. Therefore, the mass transfer benefits will be retained, and the flexibility of post-synthetic modification will allow for other binding moieties beyond amidoxime to be examined. With more promising molecular recognition moiety/functionality to be identified in the future and anchored on the membrane pore wall, this block polymer composite membrane should realize its full potential to enable the high-efficient uranium capture under trace concentrations.

CRediT authorship contribution statement

Xinping He: Conceptualization, Methodology, Investigation, Formal analysis, Writing – review & editing, Visualization. **Michael P. Dugas:** Methodology, Investigation, Formal analysis, Writing – original draft, Writing – review & editing, Visualization. **John N. Hodul:** Methodology, Investigation, Formal analysis, Writing – original draft, Writing – review & editing, Visualization. **Bryan W. Boudouris:** Conceptualization, Writing – review & editing, Funding acquisition, Supervision. **William A. Phillip:** Conceptualization, Writing – review & editing, Funding acquisition, Supervision.

Declaration of Competing Interest

The authors declare that they have no known competing financial interests or personal relationships that could have appeared to influence the work reported in this paper.

Data availability

Data will be made available on request.

Acknowledgements

This work was kindly support by the National Science Foundation (NSF) through awards 1924714 (Purdue University) and 1924715 (University of Notre Dame). We thank the NSF for this generous support. The authors would like to acknowledge the Notre Dame Center for Environmental Science and Technology (CEST) for the use of instruments to perform experiments. M.P.D. gratefully acknowledges support from the CEST/Bayer Predoctoral Fellowship.

Appendix A. Supplementary data

Supplementary data to this article can be found online at https://doi.org/10.1016/j.apsusc.2023.158650.

References

[1] K. Dungan, G. Butler, F.R. Livens, L.M. Warren, Uranium from seawater – Infinite resource or improbable aspiration? Prog. Nucl. Energy 99 (2017) 81–85, https://doi.org/10.1016/j.pnucene.2017.04.016.
[2] C.W. Abney, R.T. Mayes, T. Saito, S. Dai, Materials for the Recovery of Uranium from Seawater, Chem. Rev. 117 (2017) 13935–14013, https://doi.org/10.1021/acs.chemrev.7b00355.
[3] W. Yang, Q. Pan, S. Song, H. Zhang, Metal-organic framework-based materials for the recovery of uranium from aqueous solutions, Inorg. Chem. Front. 6 (2019) 1924–1937, https://doi.org/10.1039/c9qi00386j.
[4] Y.N. Vodyanitskii, Chemical aspects of uranium behavior in soils: A review, Eurasian Soil Sci. 44 (2011) 862–873, https://doi.org/10.1134/S1064229311080163.
[5] M. Gavrilescu, L.V. Pavel, I. Cretescu, Characterization and remediation of soils contaminated with uranium, J. Hazard. Mater. 163 (2009) 475–510, https://doi.org/10.1016/j.jhazmat.2008.07.103.
[6] J. Kim, C. Tsouris, R.T. Mayes, Y. Oyola, T. Saito, C.J. Janke, S. Dai, E. Schneider, D. Sachde, Recovery of Uranium from Seawater: A Review of Current Status and Future Research Needs, Separat. Sci. Technol. (Philadelphia) 48 (2013) 367–387, https://doi.org/10.1080/01496395.2012.712599.
[7] J.S. Wang, C.N. Sheaff, B. Yoon, R.S. Addleman, C.M. Wai, Extraction of uranium from aqueous solutions by using ionic liquid and supercritical carbon dioxide in conjunction, Chem. A Eur. J. 15 (2009) 4458–4463, https://doi.org/10.1002/chem.200801415.
[8] M. Darekar, K.K. Singh, P. Sapkale, A.K. Goswami, S. Mukhopadhyay, K.T. Shenoy, On microfluidic solvent extraction of uranium, Chem. Eng. Process. - Process Intesif. 132 (2018) 65–74, https://doi.org/10.1016/j.cep.2018.08.007.
[9] P. Li, B. Zhun, X. Wang, P. Liao, G. Wang, L. Wang, Y. Guo, W. Zhang, Highly Efficient Interception and Precipitation of Uranium(VI) from Aqueous Solution by Iron-Electrocoagulation Combined with Cooperative Chelation by Organic Ligands, Environ. Sci. Tech. 51 (2017) 14368–14378, https://doi.org/10.1021/acs.est.7b05288.
[10] M.C. Duff, J.U. Coughlin, D.B. Hunter, Uranium co-precipitation with iron oxide minerals, Geochim. Cosmochim. Acta 66 (2002) 3533–3547, https://doi.org/10.1016/S0016-7037(02)00953-5.
[11] T. Tatarchuk, A. Shyichuk, I. Mironyuk, M. Naushad, A review on removal of uranium(VI) ions using titanium dioxide based sorbents, J. Mol. Liq. 293 (2019), 111563, https://doi.org/10.1016/j.molliq.2019.111563.
[12] X. Liu, H. Liu, H. Ma, C. Cao, M. Yu, Z. Wang, B. Deng, M. Wang, J. Li, Adsorption of the uranyl ions on an amidoxime-based polyethylene nonwoven fabric prepared by preirradiation-induced emulsion graft polymerization, Ind. Eng. Chem. Res. 51 (2012) 15089–15095, https://doi.org/10.1021/ie301965g.
[13] E. Rosenberg, G. Pinson, R. Tsosie, H. Tutu, E. Cukrowska, Uranium remediation by ion exchange and sorption methods: A critical review, Johnson Matthey Technol. Rev. 60 (2016) 59–77, https://doi.org/10.1595/205651316X690178.
[14] J. Shen, A. Schäfer, Removal of fluoride and uranium by nanofiltration and reverse osmosis: A review, Chemosphere 117 (2014) 679–691, https://doi.org/10.1016/j.chemosphere.2014.09.090.
[15] O. Raff, R.D. Wilken, Removal of dissolved uranium by nanofiltration, Desalination 122 (1999) 147–150, https://doi.org/10.1016/S0011-9164(99)00035-1.
[16] P. Giridhar, K.A. Venkatesan, T.G. Srinivasan, P.R. Vasudeva Rao, Extraction of uranium(VI) from nitric acid medium by 1.1M tri-n-butylphosphate in ionic liquid diluent, J Radioanal Nucl Chem. 265 (2005) 31–38. 10.1007/s10967-005-0785-7.
[17] G.T. Campbell, M H; Frame, J M; Dudey, N D; Kiel, G R; Mesec, V; Woodfield, F W; Binney, S E; Jante, M R; Anderson, R C; Clark, Extraction of uranium from seawater: chemical process and plant design feasibility study, 1979.
[18] M. Kanno, Present status of study on extraction of uranium from sea water, J. Nucl. Sci. Technol. 21 (1984) 1–9, https://doi.org/10.1080/18811248.1984.9731004.
[19] T. Hori, M. Yamawaki, M. Kanno, Uranium adsorption properties of hydrous titanium oxides in seawater, J. Nucl. Sci. Technol. 24 (1987) 377–384, https://doi.org/10.1080/18811248.1987.9735817.
[20] L. Astheimer, H.J. Schenk, E.G. Witte, K. Schwochau, Development of Sorbers for the Recovery of Uranium from Seawater. Part 2. The Accumulation of Uranium from Seawater by Resins Containing Amidoxime and Imidoxime Functional Groups, Sep Sci Technol. 18 (1983) 307–339. 10.1080/01496398308068568.
[21] T. Kawai, K. Saito, K. Sugita, A. Katakai, N. Seko, T. Sugo, J.I. Kanno, T. Kawakami, Comparison of amidoxime adsorbents prepared by cografting methacrylic acid and 2-hydroxyethyl methacrylate with acrylonitrile onto polyethylene, Ind. Eng. Chem. Res. 39 (2000) 2910–2915, https://doi.org/10.1021/ie990474a.
[22] J. Fasihi, S. Ammari Alahyari, M. Shamsipur, H. Sharghi, A. Charkhi, Adsorption of uranyl ion onto an anthraquinone based ion-imprinted copolymer, React Funct Polym. 71 (2011) 803–808. 10.1016/j.reactfunctpolym.2011.03.014.
[23] S. Shinkai, H. Kawaguchi, O. Manabe, Selective adsorption of UO22 to a polymer resin immobilizing calixarene-based uranophiles, J. Polym. Sci., Polym. Lett. Ed. 26 (1988) 391–396.
[24] M. Carboni, C.W. Abney, S. Liu, W. Lin, Highly porous and stable metal-organic frameworks for uranium extraction, Chem. Sci. 4 (2013) 2396–2402, https://doi.org/10.1039/c3sc50230a.
[25] J. Li, X. Yang, C. Bai, Y. Tian, B. Li, S. Zhang, X. Yang, S. Ding, C. Xia, X. Tan, L. Ma, S. Li, A novel benzimidazole-functionalized 2-D COF material: Synthesis and application as a selective solid-phase extractant for separation of uranium, J. Colloid Interface Sci. 437 (2015) 211–218, https://doi.org/10.1016/j.jcis.2014.09.046.
[26] L. Ma, J. Gao, C. Huang, X. Xu, L. Xu, R. Ding, H. Bao, Z. Wang, G. Xu, Q. Li, P. Deng, H. Ma, UiO-66-NH-(AO) MOFs with a New Ligand BDC-NH-(CN) for Efficient Extraction of Uranium from Seawater, ACS Appl. Mater. Interfaces 13 (2021) 57831–57840, https://doi.org/10.1021/acsami.1c18625.
[27] M. Zhang, Q. Gao, C. Yang, L. Pang, H. Wang, H. Li, R. Li, L. Xu, Z. Xing, J. Hu, G. Wu, Preparation of Amidoxime-Based Nylon-66 Fibers for Removing Uranium from Low-Concentration Aqueous Solutions and Simulated Nuclear Industry Effluents, Ind. Eng. Chem. Res. 55 (2016) 10523–10532, https://doi.org/10.1021/acs.iecr.6b02652.
[28] W. Chouyyok, J.W. Pittman, M.G. Warner, K.M. Nell, D.C. Clubb, G.A. Gill, R. S. Addleman, Surface functionalized nanostructured ceramic sorbents for the effective collection and recovery of uranium from seawater, Dalton Trans. 45 (2016) 11312–11325, https://doi.org/10.1039/c6dt01318j.
[29] M. Hua, S. Zhang, B. Pan, W. Zhang, L. Lv, Q. Zhang, Heavy metal removal from water/wastewater by nanosized metal oxides: A review, J. Hazard. Mater. 211–212 (2012) 317–331, https://doi.org/10.1016/j.jhazmat.2011.10.016.
[30] M. Gamal Khedr, Radioactive contamination of groundwater, special aspects and advantages of removal by reverse osmosis and nanofiltration, Desalination 321 (2013) 47–54, https://doi.org/10.1016/j.desal.2013.01.013.
[31] P.S. Singh, P. Ray, A.F. Ismail, Chapter 2 - Synthetic polymer-based membranes for desalination, in: A.F. Ismail, W.N.W. Salleh, N.B.T.-S.P.M. for A.W.T. Yusof Gas Separation, and Energy Sustainability (Eds.), Elsevier, 2020: pp. 23–38. 10.1016/B978-0-12-818485-1.00002-2.
[32] A. Alblooshi, A. Giwa, D. Mukherjee, V. Calabro, A. Cassano, S. Chakraborty, S.W. Hasan, Renewable energy-powered membrane systems for water desalination, Elsevier Inc., 2018. 10.1016/B978-0-12-813545-7.00007-6.
[33] Z. Liu, F. Luo, X.J. Ju, R. Xie, Y.M. Sun, W. Wang, L.Y. Chu, Gating membranes for water treatment: Detection and removal of trace Pb2+ ions based on molecular recognition and polymer phase transition, J Mater Chem A Mater. 1 (2013) 9659–9671, https://doi.org/10.1039/c3ta12006f.
[34] N. Kubota, Y. Konno, S. Miura, K. Saito, K. Sugita, K. Watanabe, T. Sugo, Comparison of two convection-aided protein adsorption methods using porous membranes and perfusion beads, Biotechnol. Prog. 12 (1996) 869–872, https://doi.org/10.1021/bp960076s.
[35] Y. Zhang, J.R. Vallin, J.K. Sahoo, F. Gao, B.W. Boudouris, M.J. Webber, W. A. Phillip, High-A ffi nity Detection and Capture of Heavy Metal Contaminants using Block Polymer Composite, Membranes (2018), https://doi.org/10.1021/acscentsci.8b00690.
[36] Y. Wang, Y. Zhang, Q. Li, Y. Li, L. Cao, W. Li, Amidoximated cellulose fiber membrane for uranium extraction from simulated seawater, Carbohydr. Polym. 245 (2020), 116627, https://doi.org/10.1016/j.carbpol.2020.116627.
[37] S. Xie, X. Liu, B. Zhang, H. Ma, C. Ling, M. Yu, L. Li, J. Li, Electrospun nanofibrous adsorbents for uranium extraction from seawater, J Mater Chem A Mater. 3 (2015) 2552–2558, https://doi.org/10.1039/c4ta06120a.
[38] X. Lu, D. Zhang, A. Tesfay Reda, C. Liu, Z. Yang, S. Guo, S. Xiao, Y. Ouyang, Synthesis of Amidoxime-Grafted Activated Carbon Fibers for Efficient Recovery of Uranium(VI) from Aqueous Solution, Ind. Eng. Chem. Res. 56 (2017) 11936–11947, https://doi.org/10.1021/acs.iecr.7b02690.
[39] V.P. Khare, A.R. Greenberg, W.B. Krantz, Vapor-induced phase separation - Effect of the humid air exposure step on membrane morphology: Part I. Insights from Mathematical Modeling, J Memb Sci. 258 (2005) 140–156, https://doi.org/10.1016/j.memsci.2005.03.015.

[40] G.R. Guillen, Y. Pan, M. Li, E.M.V. Hoek, Preparation and characterization of membranes formed by nonsolvent induced phase separation: A review, Ind. Eng. Chem. Res. 50 (2011) 3798–3817, https://doi.org/10.1021/ie101928r.
[41] H. Chae Park, Y. Po Kim, H. Yong Kim, Y. Soo Kang, Membrane formation by water vapor induced phase inversion, J Memb Sci. 156 (1999) 169–178, https://doi.org/10.1016/S0376-7388(98)00359-7.
[42] S.P. Nunes, Block copolymer membranes, in: Sustainable Nanoscale Engineering: From Materials Design to Chemical Processing, Elsevier, 2019: pp. 297–316. 10.1016/B978-0-12-814681-1.00011-4.
[43] K.V. Peinemann, V. Abetz, P.F.W. Simon, Asymmetric superstructure formed in a block copolymer via phase separation, Nat. Mater. 6 (2007) 992–996, https://doi.org/10.1038/nmat2038.
[44] F.J. Tsai, J.M. Torkelson, Roles of phase separation mechanism and coarsening in the formation of poly(Methyl methacrylate) asymmetric membranes, Macromolecules 23 (1990) 775–784, https://doi.org/10.1021/ma00205a014.
[45] L.P. McMaster, Aspects of liquid-liquid phase transition phenomena in multicomponent polymeric systems, Adv. Chem. Ser. (1975) 43–65, https://doi.org/10.1021/ba-1975-0142.ch005.
[46] 丁耀莹, 王成志, 问县芳, 张鑫鹏, 叶霖, 张爱英, 冯增国, 偕胺肟化聚丙烯腈纳米纤维的制备及在含金属离子废水处理中的应用, 高等学校化学学报. 34 (2013) 1758–1764.
[47] M. Ruiz-Bermejo, P. García-Armada, E. Mateo-Martí, J.L. de la Fuente, HCN-derived polymers from thermally induced polymerization of diaminomaleonitrile: A non-enzymatic peroxide sensor based on prebiotic chemistry, Eur. Polym. J. 162 (2022), https://doi.org/10.1016/j.eurpolymj.2021.110897.
[48] J. Wu, K. Tian, J. Wang, Adsorption of uranium (VI) by amidoxime modified multiwalled carbon nanotubes, Prog. Nucl. Energy 106 (2018) 79–86, https://doi.org/10.1016/j.pnucene.2018.02.020.
[49] J.L. Weidman, R.A. Mulvenna, B.W. Boudouris, W.A. Phillip, Unusually Stable Hysteresis in the pH-Response of Poly(Acrylic Acid) Brushes Con fi ned within Nanoporous Block Polymer Thin Films, (2016). 10.1021/jacs.6b01618.
[50] Y. Zhang, R.A. Mulvenna, S. Qu, B.W. Boudouris, W.A. Phillip, Block Polymer Membranes Functionalized with Nanocon fi ned Polyelectrolyte Brushes Achieve Sub-Nanometer Selectivity, (2017). 10.1021/acsmacrolett.7b00278.
[51] J. Wang, X. Guo, Adsorption isotherm models: Classification, physical meaning, application and solving method, Chemosphere 258 (2020), 127279, https://doi.org/10.1016/j.chemosphere.2020.127279.
[52] Q.Y. Wu, J.H. Lan, C.Z. Wang, C.L. Xiao, Y.L. Zhao, Y.Z. Wei, Z.F. Chai, W.Q. Shi, Understanding the bonding nature of uranyl ion and functionalized graphene: A theoretical study, J. Phys. Chem. A 118 (2014) 2149–2158, https://doi.org/10.1021/jp500924a.
[53] Y. Sun, S. Yang, Y. Chen, C. Ding, W. Cheng, X. Wang, Adsorption and desorption of U(VI) on functionalized graphene oxides: A combined experimental and theoretical study, Environ. Sci. Tech. 49 (2015) 4255–4262, https://doi.org/10.1021/es505590j.
[54] C.Z. Wang, J.H. Lan, Q.Y. Wu, Q. Luo, Y.L. Zhao, X.K. Wang, Z.F. Chai, W.Q. Shi, Theoretical insights on the interaction of uranium with amidoxime and carboxyl groups, Inorg. Chem. 53 (2014) 9466–9476, https://doi.org/10.1021/ic500202g.
[55] G.M. Marion, F.J. Millero, M.F. Camões, P. Spitzer, R. Feistel, C.T.A. Chen, PH of seawater, Mar. Chem. 126 (2011) 89–96, https://doi.org/10.1016/j.marchem.2011.04.002.
[56] Y. Wang, Z. Gu, J. Yang, J. Liao, Y. Yang, N. Liu, J. Tang, Amidoxime-grafted multiwalled carbon nanotubes by plasma techniques for efficient removal of uranium(VI), Appl. Surf. Sci. 320 (2014) 10–20, https://doi.org/10.1016/j.apsusc.2014.08.182.
[57] Y. Zhao, J. Li, L. Zhao, S. Zhang, Y. Huang, X. Wu, X. Wang, Synthesis of amidoxime-functionalized Fe3O4@SiO2 core-shell magnetic microspheres for highly efficient sorption of U(VI), Chem. Eng. J. 235 (2014) 275–283, https://doi.org/10.1016/j.cej.2013.09.034.
[58] J. Kim, C. Tsouris, Y. Oyola, C.J. Janke, R.T. Mayes, S. Dai, G. Gill, L.J. Kuo, J. Wood, K.Y. Choe, E. Schneider, H. Lindner, Uptake of uranium from seawater by amidoxime-based polymeric adsorbent: Field experiments, modeling, and updated economic assessment, Ind. Eng. Chem. Res. 53 (2014) 6076–6083, https://doi.org/10.1021/ie4039828.
[59] Q. Gao, J. Hu, R. Li, Z. Xing, L. Xu, M. Wang, X. Guo, G. Wu, Radiation synthesis of a new amidoximated UHMWPE fibrous adsorbent with high adsorption selectivity for uranium over vanadium in simulated seawater, Radiat. Phys. Chem. 122 (2016) 1–8, https://doi.org/10.1016/j.radphyschem.2015.12.023.
[60] J.W. Moffett, R.G. Zika, Solvent extraction of copper acetylacetonate in studies of copper(II) speciation in seawater, Mar. Chem. 21 (1987) 301–313, https://doi.org/10.1016/0304-4203(87)90053-3.
[61] B. Aguila, Q. Sun, H. Cassady, C.W. Abney, B. Li, S. Ma, Design Strategies to Enhance Amidoxime Chelators for Uranium Recovery, ACS Appl. Mater. Interfaces 11 (2019) 30919–30926, https://doi.org/10.1021/acsami.9b09532.
[62] Y. Li, Y. Dai, Z. Gao, Z. Li, F. He, L. Xu, Q. Tao, Adsorption of uranium onto amidoxime-group mesoporous biomass carbon: kinetics, isotherm and thermodynamics, J. Radioanal. Nucl. Chem. 331 (2022) 353–364, https://doi.org/10.1007/s10967-021-08115-x.
[63] M. Stephan, D. Pospiech, R. Heidel, T. Hoffmann, D. Voigt, H. Dorschner, Electron beam irradiation of molten polysulfone, in: Polym Degrad Stab, Elsevier Ltd, 2005: pp. 379–385. 10.1016/j.polymdegradstab.2005.04.049.
[64] A. Bedar, B.G. Singh, P.K. Tewari, R.C. Bindal, S. Kar, Kinetics studies on free radical scavenging property of ceria in polysulfone-ceria radiation resistant mixed-matrix membrane, Int. J. Chem. React. Eng. 19 (2021) 779–785, https://doi.org/10.1515/ijcre-2020-0123.
[65] A. Bedar, R.K. Lenka, N. Goswami, V. Kumar, A.K. Debnath, D. Sen, S. Kumar, S. Ghodke, P.K. Tewari, R.C. Bindal, S. Kar, Polysulfone-Ceria Mixed-Matrix Membrane with Enhanced Radiation Resistance Behavior, ACS Appl Polym Mater. 1 (2019) 1854–1865, https://doi.org/10.1021/acsapm.9b00389.